# Mechanism of Efficient Adsorption of Na Atoms on Electron-Deficient Doped $MoS_2$ for Battery Electrodes

Yudong Pang,[1] Zhansheng Lu,[1,†] Shamraiz Hussain Talib,[1,2] Xinyuan Li,[1] Mingyang Wang,[1] Xilin Zhang,[1] Zongxian Yang,[1,*] and Ruqian Wu[3,‡]

[1] *School of Physics, Henan Normal University and Henan Key Laboratory of Photovoltaic Materials, Xinxiang, Henan 453007, People's Republic of China*

[2] *Department of Chemistry and Key Laboratory of Organic Optoelectronics & Molecular Engineering of Ministry of Education, Tsinghua University, Beijing 100084, People's Republic of China*

[3] *Department of Physics & Astronomy, University of California, Irvine, California 92697, USA*

(Received 7 April 2022; revised 20 June 2022; accepted 8 July 2022; published 22 September 2022)

Due to the similarities in electrochemical and physicochemical properties of sodium and lithium, sodium-ion batteries are an attractive substitute for lithium-ion batteries. The selection of appropriate electrode materials for Na-ion batteries is an important step to achieve high stability and theoretical capacity. Here, the effects of heteroatom doping and charge variation on the ability of the $MoS_2$ substrate to capture Na ions are studied using first-principles calculations. The results show that the interaction between Na ions and the $MoS_2$ substrate is enhanced by electron deficiency or substituting a S atom with a dopant atom ($X$) with fewer valence electrons ($X$ = B, Al, Ga, In, C, Si, Ge, Sn, N, P, As, Sb). In contrast, adding electrons to the $MoS_2$ substrate weakens its interaction with Na. We further analyze the diffusion barrier, open-circuit voltage, and theoretical capacity of hypothetical Na-ion batteries using doped $X$-$MoS_2$ ($X$ = heteroatom) as electrode materials. We find that Al- or Si-doped $MoS_2$ can serve as good electrode materials for Na-ion batteries, with a high theoretical capacity that exceeds 700 mAh/g. This work provides practical guidance for the development of electrode materials of Na-ion batteries using two-dimensional materials.

DOI: 10.1103/PhysRevApplied.18.034061

## I. INTRODUCTION

Lithium-ion batteries (LIBs) are widely used in rechargeable automobiles, portable electronics, and energy storage due to their high power density as well as high energy density. However, due to the limited availability and unequal distribution of global lithium resources, the cost of LIBs constantly increases. In the meantime, they still have inherent technical issues, such as poor low-temperature performance and inadequate safety protection. Currently, interdisciplinary efforts are dedicated to developing batteries with metal ions that may offer low cost, environmental friendliness, and a high theoretical capacity. Among various potential candidates, sodium-ion batteries (SIBs) have attracted considerable attention, as they have very similar properties to Li-ion batteries but with lower cost and better safety [1–4]. Sodium is the next-smallest alkali metal and has a larger size than Li. A critical challenge for the development of Na-ion batteries is to find appropriate electrode and electrolyte materials that may provide a large adsorption capacity, high mobility, and strong support for Na ions. To this end, the target materials must have an adequate grasp on Na ions, shallow barrier for their segregation, and strong structural stability.

Recently, many two-dimensional (2D) materials without and with modification by heteroatoms have been investigated as potential electrode materials for metal-ion batteries [5–16]. For example, graphene proves to be a superior electrode material for Li-ion batteries with high theoretical capacity [5,8,17,18]. However, the ionic radius of Na (1.06 Å) is larger than that of Li (0.76 Å), and the adsorption and diffusion kinetics of Na ions in graphene layers are somewhat limited [19–21]. To improve this scenario, Qiao *et al*. report that phosphorus doping in graphene may increase the interlayer spacing, and hence, enhance the adsorption and migration of Na ions between graphene layers [22]. They also report that the coupling between $MoS_2$ and nitrogen-doped graphene layers considerably enhances the adsorption capacity of Na ions [23]. Kavalsky and coworkers investigated the adsorption of Na ions on the blue phosphorus and found that this material had a high capacity for hosting alkali ions and high K and Na diffusivity [24]. Several types of heteroatom- (e.g., Si- [16], Ge- [9], and C- [12]) doped blue phosphorus are widely explored, and they

*yzx@htu.edu.cn
†zslu@htu.edu.cn
‡wur@uci.edu

 

are one of the top candidates for the design of battery materials. Recent studies further specify that pentagraphene as a substrate has a much higher theoretical capacity of Na or Li ions [25] compared with other 2D electrode materials. Cheng *et al.* report that B-doped pentagraphene may have an even higher theoretical capacity for Na- or Li-ion batteries than pristine pentagraphene [14]. Barik and Pal report that the presence of S and Mo vacancies may improve the Na-adsorption capacity and diffusion abilities of $MoS_2$ [26]. Feng *et al.* report that substituting Se with P in three-dimensional $CoSe_2$ enhances its theoretical Li capacity [27]. Ni *et al*. report that introducing oxygen vacancies leads to excellent performance of $TiO_2$ as an electrode material for Na-ion batteries [28]. From these prior studies, it is established that doped or defect materials are more suitable electrode materials for metal-ion batteries. In particular, this is a critical strategy to improve the performance of sodium-ion batteries by overcoming problems such as low capacity and poor initial Coulombic efficiency.

Here, we investigate how to engineer 2D $MoS_2$-based materials as electrodes in Na-ion batteries through systematic density-functional theory (DFT) calculations. Among popular 2D materials, $MoS_2$ is a van der Waals (vdW) type layered material [29] that is explored for a varity of applications, such as energy storage, optoelectronics, and spintronics. However, pure $MoS_2$ is not suitable as an electrode material for Na-ion batteries, as it has a large band gap, and hence, a weak interaction with Na [30]. To find out if heteroatoms can activate $MoS_2$, we perform systemic studies for the adsorption and segregation of Na on doped $MoS_2$ monolayer ($X$-$MoS_2$, $X = $B, Al, Ga, In, C, N, Si, Ge, Sn, N, P, As, Sb, O, Se, Te, F, Cl, Br, I). We first examine structural stability, ground-state electronic properties, and adsorption of Na ions of pure and N-doped $MoS_2$ (N-$MoS_2$) monolayer. To reveal the mechanisms, the charged systems of pure and N-doped $MoS_2$ are studied with electron extraction or injection. Finally, we investigate the important parameters for electrode materials, such as diffusion barrier, theoretical capacity, and open-circuit voltage, which primarily depend on the number of Na atoms on the substrate. We find that electron extraction from the $MoS_2$ substrate or substitution of a S atom of $MoS_2$ with a dopant that has fewer valence electrons increases the interaction between Na and $MoS_2$, resulting in a higher adsorption energy. We predict that the Al- or Si-$MoS_2$ systems can serve as good electrode materials for Na-ion batteries with a high theoretical capacity and high performance.

## II. COMPUTATIONAL DETAILS

Using the Vienna *ab initio* simulation package [31,32] with the projected-augmented-wave approach [33], the first-principles calculations are performed based on the spin-polarized DFT at the level of the generalized gradient approximation with the Perdew-Burke-Ernzerhof functional [34]. The vdW interaction is included using the DFT-D3 method [35,36]. The plane-wave cutoff is set as 500 eV, and the threshold convergence for energy is set at $1 \times 10^{-5}$ eV. Structural relaxation is pursued until the maximum force is less than 0.02 eV Å$^{-1}$. To investigate Na adsorption on the $X$-$MoS_2$ substrates ($X = $B, Al, Ga, In, C, N, Si, Ge, Sn, N, P, As, Sb, O, Se, Te, F, Cl, Br, I), a single layer of $MoS_2$ with a $4 \times 4$ replication in the $x$-$y$ plane and a vacuum layer of more than 15 Å along the $z$ direction is used to mimic the substrate, as presented in Fig. 1(a). The Brillouin zone is sampled with a $3 \times 3 \times 1$ Monkhorst-Pack $k$-point mesh for geometrical optimization and with a $5 \times 5 \times 1$ $k$ mesh for electronic structure calculations [37]. The charge transfer of doped systems is analyzed using Bader's quantum theory of atoms in molecules (QTAIM) [38,39]. The charge-accumulation and -depletion regions can be visualized through charge-density differences (CDDs $= \rho_{AB} - \rho_A - \rho_B$, with $\rho_{AB}$, $\rho_A$, and $\rho_B$ representing the charge densities of combined and separated systems). Furthermore, the average adsorption energies ($E_{ads}$) for Na on the substrate are obtained from

$$E_{ads} = (\lambda E_{Na} + E_{substrate} - E_{\lambda Na + substrate})/\lambda. \quad (1)$$

Here, $E_{Na}$, $E_{substrate}$, and $E_{\lambda Na+substrate}$ represent the energy of a Na atom in the bulk Na metal, the energy of the substrate, and the energy of the substrate with $\lambda$ Na adatoms, respectively. According to this definition, the greater the value of $E_{ads}$, the stronger the interaction between Na and the substrate. The climbing-image nudged elastic band (CINEB) method [40], with four mirror images inserted between the initial- and final-state structures, is used to search for the diffusion barriers. The energy and atomic force convergence threshold settings for CINEB are the same as those for structural optimization.

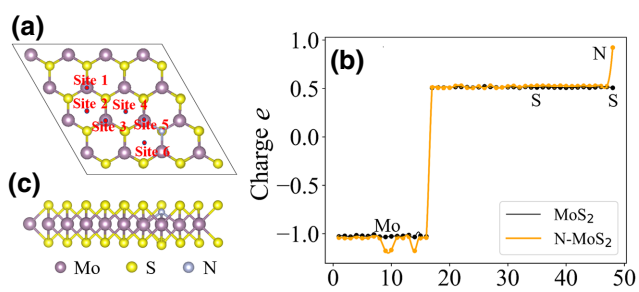


FIG. 1. (a),(b) Top and side views of N-$MoS_2$ substrate, with different adsorption sites (red dots) for the Na atom (site 1–site 6). (c) Bader charges of $MoS_2$ and N-$MoS_2$. Positive value represents gain of electrons. Numbers on the $x$ axis show the labels (1–16 for Mo and 17–48 for S and N) of the atoms in our model.

The open-circuit voltage ($V_{OC}$) is calculated from $E_{ads}$ by

$$V_{OC} = E_{ads}/e, \tag{2}$$

where $e$ is the charge of an electron. The theoretical storage capacity ($C$) is calculated by

$$C = xF/M_{substrate}, \tag{3}$$

where $x$ represents the maximum number of adsorbed Na atoms on the substrate, F is the Faraday constant (F = 26.8 Ah/mol), and $M_{substrate}$ is the molecular mass of the substrate.

## III. RESULTS AND DISCUSSION

### A. The geometric and electronic properties of $MoS_2$ and N-$MoS_2$

Since the $MoS_2$ structure of the 2$H$ phase is more stable than that of the 1$T$ phase, here we choose the 2$H$-phase structure as the model for research. In this work, the 2$H$-phase $MoS_2$ monolayer is chosen as the template and different heteroatoms (B, Al, Ga, In, C, N, Si, Ge, Sn, N, P, As, Sb, O, Se, Te, F, Cl, Br, I) are used as dopants for substituting the S atoms. Among them, N-$MoS_2$ is studied experimentally and it is found that the Mo—N bonds are strong in N-$MoS_2$ [23]. Accordingly, we first study the geometric and electronic properties of N-$MoS_2$ and compared them with those of the pristine $MoS_2$ monolayer. The top and side views of the optimized configuration of N-$MoS_2$ are presented in Figs. 1(a) and 1(b). It is found that, in the optimized structure of N-$MoS_2$, the N—Mo bond length (2.04 Å) is considerably shorter than the S—Mo bond (2.41 Å), signifying that there is a strong interaction between the N and Mo. Figure 1(c) depicts the charge-distribution comparison between the $MoS_2$ and N-$MoS_2$ substrates. The Bader charge analysis further confirms the strong interaction between N and $MoS_2$. In the pristine $MoS_2$ monolayer, each Mo atom transfers 1 $|e|$ and each S atom gains 0.5 $|e|$. In N-$MoS_2$, the Mo atoms nearest to N donate more electrons (approximately 1.2 $|e|$) to the N atom, and the N atom gains 0.9 $|e|$ from its neighbors [see Fig. 1(c)]. The larger electronegativity of N (3.04) compared with that of S (2.58) explains this extra electron gain and implies stronger binding between N and Mo than that between S and Mo.

### B. The adsorption of Na on $MoS_2$ and N-$MoS_2$

Next, we investigate the adsorption of Na over the N-$MoS_2$ substrate. The structure of the N-$MoS_2$ substrate has low symmetry and Na ions are likely to adsorb at six different sites [see Fig. 1(a)]. There are two different kinds of adsorption sites. Site 1, site 3, and site 5 are located directly above the Mo atom, while site 2, site 4, and site 6 are located in the hollow sites of $MoS_2$. Their positions and distances relative to dopant $X$ can be seen from the top view of the structure. The calculated adsorption energies and the Na-substrate average distances are listed in Table I, along with corresponding values for Na on pristine $MoS_2$. As expected, the absorption of Na on pure $MoS_2$ is very weak, with an adsorption energy of only 0.13 eV. In contrast, the adsorption energies of Na over the N-$MoS_2$ substrate at different adsorption sites are consistently high, 1.45 to 2.12 eV. The significant increase in adsorption energy can be attributed to the change of local chemistry of N-$MoS_2$. As shown in Table I, stable adsorption sites for Na are around the top of Mo (sites 5 and 6) near N, and the adsorption energy is as high as 2.12 eV. Obviously, the ability of $MoS_2$ to host Na atoms is significantly improved by N doping. Furthermore, we find that strong adsorption of Na correlates well with the average distance between the Na ion and N-$MoS_2$ substrate [see Table I]. To further explore the origin of the strong interaction between Na and the N-$MoS_2$ substrate, Figs. 2(ai) and 2(aii) gives the Bader charges for Na/N-$MoS_2$ in all possible adsorption configurations. It is clear that the Na atom close to the doped N atom site loses more electrons than those at the other adsorption sites. We may conclude that electron transfer from Na to N is primarily responsible for the enhanced interaction between Na and N-$MoS_2$.

### C. The mechanism for the enhancement of Na adsorption on N-$MoS_2$

To further explore the adsorption properties of Na over the N-$MoS_2$ substrate, the CDDs are presented in Figs. 2(b) and 2(g). These results show a substantial charge reduction around the Na atom at site 5 and site 6, and charge accumulation around the N atom nearby, in good correspondence with the Bader charge analysis. Since N has one less valence electron than S, doping N into $MoS_2$ generates an electron-deficient system, and hence, N-$MoS_2$

TABLE I. Adsorption energies ($E_{ads}$) and Na-substrate average distance ($d_{av}$) for Na ions at different adsorption sites over the $MoS_2$ and N-$MoS_2$ substrates.

| | N-$MoS_2$ | | | | | | Pure |
|---|---|---|---|---|---|---|---|
| | Site 1 | Site 2 | Site 3 | Site 4 | Site 5 | Site 6 | $MoS_2$ |
| $E_{ads}$ (eV) | 1.467 | 1.453 | 1.517 | 1.503 | 2.120 | 2.118 | 0.126 |
| $d_{av}$ (Å) | 2.73 | 2.75 | 2.73 | 2.73 | 2.23 | 2.23 | 2.76 |

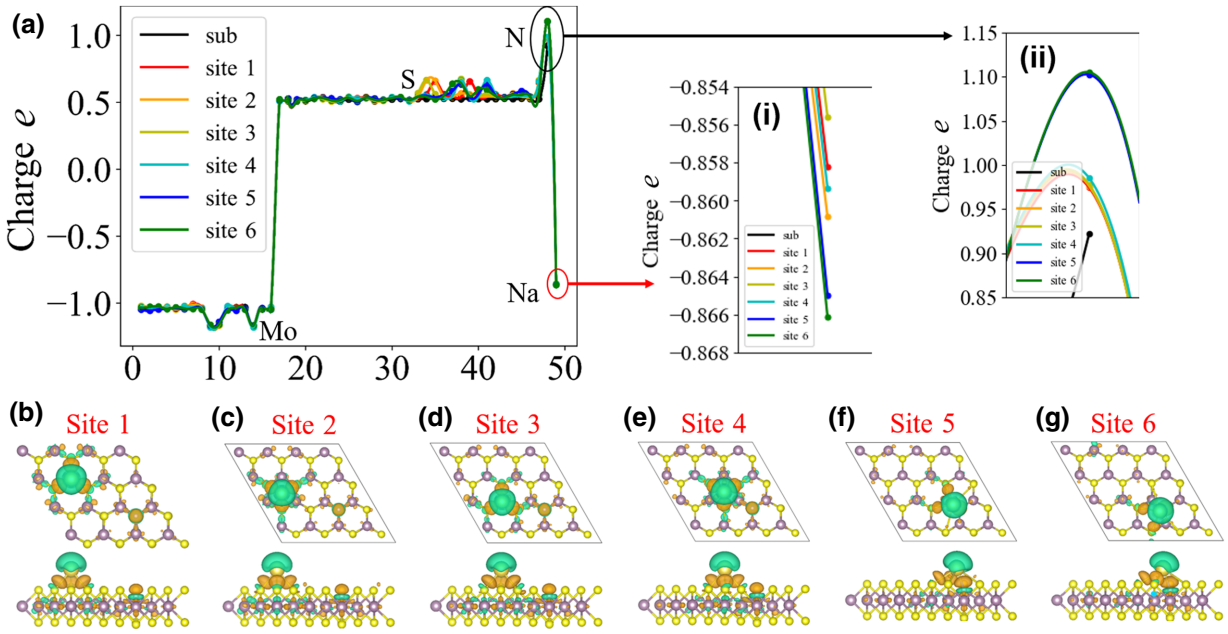


FIG. 2. (a) Bader charge analysis of Na atom adsorbed at different adsorption sites on the N-$MoS_2$ substrate. Numbers on the $x$ axis show the labels of the atoms in the model. (b)–(g) CDD analysis of Na adsorbed at different sites on the N-$MoS_2$ substrate. For contour plots, the green region represents charge depletion, and the orange region represents charge accumulation. Isosurface value of the CDDs is 0.002 e/Å$^3$.

may easily take the valence electron from Na. In this section, we analyze the effect of charge deficiency on the adsorption of Na on $MoS_2$ and N-$MoS_2$ substrates by extracting (injecting) electrons from (into) both systems. We first extract an electron from the pristine $MoS_2$ monolayer and observe its effect on the Na-adsorption ability. Figure 3(a) shows the Bader charge distribution of $MoS_2$ before and after electron extraction. After extracting an electron from the $MoS_2$ substrate, the Bader charges of the S atoms are slightly reduced. Figures 3(b), 3(c), 7(a), and 7(b) (Appendix) illustrate the Bader charges and CDDs of Na/$MoS_2$ with or without electron extraction.

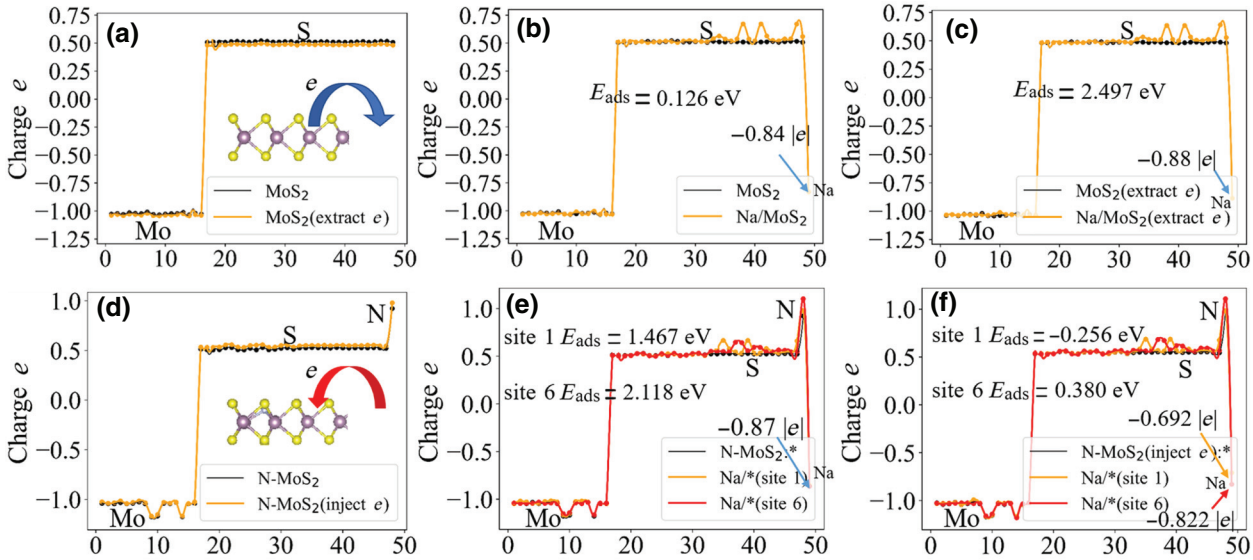


FIG. 3. (a) Bader charge analysis for electrons extracted from the pure $MoS_2$ substrate. (b) Charge variation of Na/$MoS_2$. (c) Charge variation of Na/$MoS_2$ (extract $e$). (d) Electrons injected in the N-$MoS_2$ substrate. (e) Charge variation of Na/N-$MoS_2$. (f) Charge variation of Na/N-$MoS_2$ (inject $e$). Numbers on the $x$ axis show the labels of the atoms in the model.

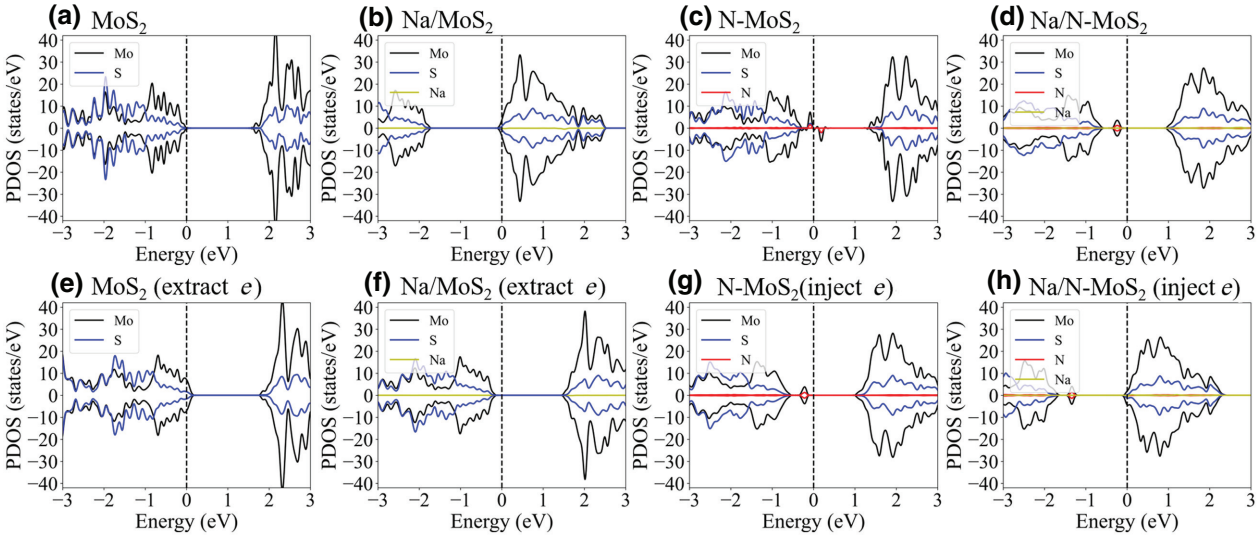


FIG. 4. PDOS for Na adsorption on the $MoS_2$ and N-$MoS_2$ substrates. (a) PDOS of the $MoS_2$ system. (b) PDOS of Na adsorption on the $MoS_2$ system. (c) PDOS of the N-$MoS_2$ substrate. (d) PDOS of Na adsorption on the N-$MoS_2$ substrate. (e) PDOS of the $MoS_2$ (extract $e$) substrate. (f) PDOS of Na adsorption on the $MoS_2$(extract $e$) substrate. (g) PDOS of the N-$MoS_2$ (inject $e$) substrate. (h) PDOS of Na adsorption on the N-$MoS_2$ (inject $e$) substrate.

The results show that the Na atom loses additional 0.04 $|e|$ due to extraction of an electron from Na/$MoS_2$. Interestingly, the adsorption energy of Na becomes 2.50 eV, around 19 times more than that on $MoS_2$ without electron extraction. This evolution is in accordance with the expectation that the electron-deficient $MoS_2$ substrate enhances the interaction between Na and $MoS_2$.

On the other hand, we may expect that a dopant introducing additional electrons into the system weakens Na adsorption. To check this conjecture, we inject an electron into the N-$MoS_2$ system and observe the interaction between Na and the N-$MoS_2$ substrate. Figure 3(d) clearly shows that, when an electron is injected into the N-$MoS_2$ system, the charge distribution of the N-$MoS_2$ (injected $e$) system is slightly changed compared with that of N-$MoS_2$, e.g., the numbers of electrons that S and N atoms gain slightly increase. Figures 3(e), 3(f), and 7(c)–7(f) (Appendix) show the Bader charges and CDDs of Na on the N-$MoS_2$ substrate with and without electron injection. When Na is adsorbed at site 1 (site 6) on the N-$MoS_2$ (inject $e$) substrate, the Bader charge analysis shows that the Na atom loses fewer electrons to the substrate by 0.05 $|e|$ (0.17 $|e|$) compared with that on N-$MoS_2$ without electron injection. The adsorption energy of Na at site 6 on the N-$MoS_2$ (inject $e$) substrate is reduced to 0.38 eV, approximately 6 times less than that on the N-$MoS_2$ substrate (2.12 eV). The negative adsorption energy of Na at site 1, which is far away from N, means that Na cannot be stably adsorbed. According to the analyses above, we may conclude that the electron-deficient $MoS_2$-based systems (e.g., N-$MoS_2$) are beneficial for Na adsorption, while dopants with excess valence electrons weaken Na adsorption.

Figure 4(a) shows the partial density of states (PDOS) of the pure $MoS_2$ substrate, where the Fermi level is in the forbidden band and the band gap is about 1.7 eV. As confirmed in Fig. 4(b), it is clear that the PDOS peak of the Na/$MoS_2$ system is downshifted due to Na adsorption. Because the Fermi level is in the forbidden band, the electron transferred from Na needs to occupy states at the conduction-band minimum, a status that is unfavorable. In addition, we also present the PDOS for N-$MoS_2$ in Fig. 4(c) and PDOS for Na adsorption on the N-$MoS_2$ substrate in Fig. 4(d). In Fig. 4(c), the doped N atom on $MoS_2$ has empty half-filled orbitals near the Fermi level. When Na is adsorbed on the N-$MoS_2$ substrate, the electron transfers from Na to the empty orbitals near the Fermi level, which is clearly seen in Fig. 4(d). It is noteworthy that electron transfer from Na to N-$MoS_2$ is much easier than that to pure $MoS_2$, resulting in a stronger interaction between Na and N-$MoS_2$.

To further clarify why Na is more strongly adsorbed on N-$MoS_2$, the PDOS of the systems with Na adsorbed on the charged $MoS_2$ and N-$MoS_2$ substrates are analyzed. It is noteworthy that, when an electron is extracted from the $MoS_2$ system, the Fermi level moves to the left, leaving an empty state near the Fermi level, as shown in Fig. 4(e). When the Na atom is adsorbed on the $MoS_2$ (extract $e$) substrate, the electron from Na may easily fill this empty state, as shown in Fig. 4(f). Likewise, when electrons are injected into N-$MoS_2$, the empty band near the Fermi level is completely filled [see Fig. 4(g)]. The electron from Na

hence has to occupy the high-energy empty states in the conduction band [see Fig. 4(h)].

### D. Potential efficient $MoS_2$-based electrode materials for Na-ion batteries

Based on the analyses above, systems with empty states near the Fermi level are suitable for the adsorption of Na. This can be further confirmed by examining the properties of $MoS_2$ with different heteroatoms (X), from groups IIIA to VIIA (X = B, Al, Ga, In, C, Si, Ge, Sn, N, P, As, Sb, O, Se, Te, F, Cl, Br, I). The stability of the X-$MoS_2$ structures is discussed in the Appendix. As shown in Fig. 8 (Appendix), the adsorption energies of Na on the X-$MoS_2$ substrate with electron-deficient dopants (X = B, Al, Ga, In, C, Si, Ge, Sn, N, P, As, Sb) are enhanced [see Table II in the Appendix], while the adsorption energies of Na on X-$MoS_2$ for the isoelectronic dopants (X = O, Se, Te) are very close to that on pristine $MoS_2$. These results stem from the reasons discussed above, as similar behavior can be seen from the PDOS of Na/$X$-$MoS_2$ in Fig. 9 (Appendix). In contrast, it is seen that the X-$MoS_2$ substrates with electron-rich group-VIIA dopants (X = F, Cl, Br, and I) have a moderate adsorption strength to Na. However, our test calculations show that the relaxed structures shown in Fig. 10 (Appendix) indicate that the strong interaction between the dopants of F, Cl, Br, and I with Na result in the precipitation of these dopant atoms from the dopant sites on the $MoS_2$ substrate upon adsorption of multiple Na ions with a concentration of Na:$MoS_2$ of 1:1. This is extremely disadvantageous for the stability of the structure and is not the case for $MoS_2$ doped with other dopant atoms, as also shown in Fig. 10 (Appendix). Therefore, electron-rich group-VIIA elements are not appropriate dopants in the $MoS_2$ substrate for the development of electrode materials for Na-ion batteries.

Generally, the diffusion barrier of Na on the substrate is another most important parameter for the performance of electrode materials. The diffusion properties of Na on the heteroatom-doped X-$MoS_2$ systems are closely associated with their rate capability, and small diffusion barriers are obligatory for electrode materials. Based on the adsorption sites and structural symmetry, the two most possible diffusion paths (path 1, site 1 → site 2 → site 3 → site 4; path 2, site 1 → site 4) are selected to study Na diffusion on pure $MoS_2$ or on the clean part (the region far away from the doped X atoms) of doped X-$MoS_2$. Na diffusion near the dopant is selected to study the effect of the dopant on Na diffusion (path 3, site 4 → site 5). The calculated energy profiles and optimized structures for Na-atom diffusion on the N-$MoS_2$ substrate are presented in Figs. 5, 11, and 12 (Appendix). Figures 5(a) and 5(b) show the Na diffusion routes via path 1 and path 2 on the clean part of N-$MoS_2$, from which we find diffusion barriers of about 0.1 eV (0.4 eV) via path 1 (path 2) [see Figs. 5(c) and 5(d)], with path 1 being kinetically more favorable. This result is similar to the diffusion of Na on the $MoS_2$ substrate, see Fig. 11 (Appendix). However, Na diffusion near the N dopant (path 3, site 5 → site 4) is required to overcome a barrier of 0.68 eV [see Fig. 12(c) in the Appendix]. Although the N-$MoS_2$ substrate improves the adsorption strength of Na on the substrate, it decreases the diffusion ability of Na near the stable site near the doping site. In addition, the diffusion of Na on the other heteroatom systems is also studied in this work, and the computed geometries and potential-energy profiles are summarized in Fig. 13 (Appendix) and Table III (Appendix). By comparing Na diffusion on the N-$MoS_2$ substrate, we find that Na diffusion on the X-$MoS_2$ (X = C, P, Ge, Ga, B) substrates has similar properties to that on the N-$MoS_2$ substrate. In these systems, the Na ions can easily diffuse to the site close to the dopant (e.g., from site 4 to site 5) with a small diffusion barrier. However, inverse diffusion away from the doping site (from site 5 to site 4) has larger energy barriers (>0.2 eV). Thus, these systems are not appropriate as electrode materials. In contrast, the diffusion barriers of Na from site 4 to site 5 and from site 5 to site 4 on the X-$MoS_2$ ($X$ = As, Si, Al) substrates are relatively close and small, with diffusion barriers less than 0.1 eV. Obviously, if the X-$MoS_2$ substrate makes the adsorption strength of Na at each position on the substrate surface more even, then the potential barriers of forward and backward diffusion of Na on these materials are similar, which makes the insertion and removal of Na easier. Therefore, these systems have a superb ion-diffusion ability and would be suitable electrode materials.

Additional important parameters for electrode materials are the theoretical capacity and open-circuit voltage, which primarily depend upon the amount of Na atoms adsorbed on the substrates. The calculated step diagrams (C-$V$ diagram) of theoretical capacity and open-circuit voltage

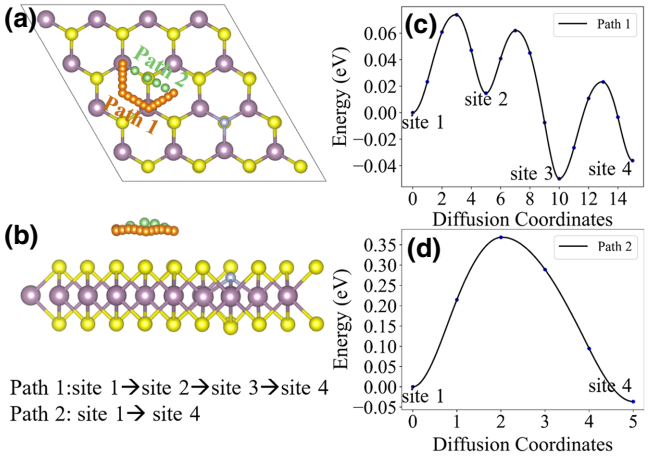


FIG. 5. (a),(b) Top and side views of Na-diffusion paths on the N-$MoS_2$ substrate. (c) Energy profile for Na diffusion via path 1. (d) Energy profile for Na diffusion via path 2.

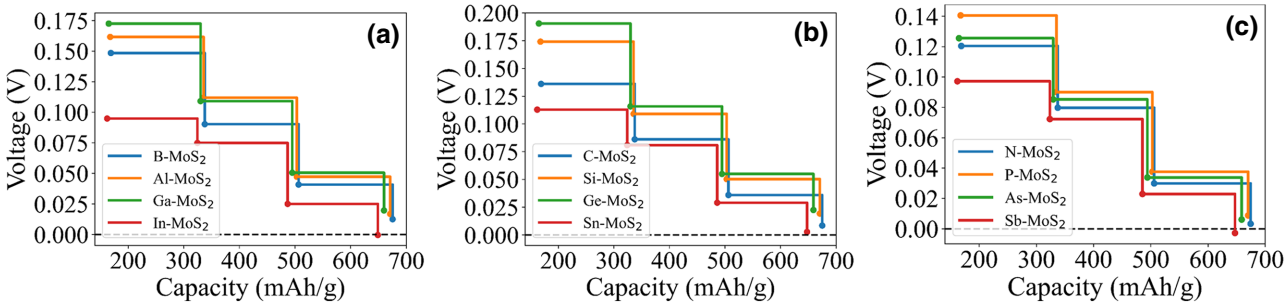


FIG. 6. Step diagrams of theoretical capacity ($C$) and average open-circuit voltage ($V_{OC}$) of multiple Na adsorption on the $X$-$MoS_2$ substrates ($X$ = heteroatoms). (a) $C$-$V$ diagram of group-IIIA-element-doped $MoS_2$. (b) $C$-$V$ diagram of group-IVA-element-doped $MoS_2$. (c) $C$-$V$ diagram of group-VA-element-doped $MoS_2$.

of the Na atom adsorbed on the X-$MoS_2$ substrates are presented in Fig. 6. Like $MoS_2$, X-$MoS_2$ (X = O, Se, and Te) has a weak adsorption ability for Na atoms, and thus, they will have poor theoretical capacities. Therefore, the $MoS_2$ substrates doped with the group-VIA element are not further discussed. Figure 6 depicts the relationship between theoretical capacity and open-circuit voltage for the doped substrates of X-$MoS_2$ with dopants from groups IIIA to VA. As seen in Fig. 6(a), for the X-$MoS_2$ systems with the group-IIIA-dopant elements (B, Al, Ga, In), the theoretical capacity shows a good relationship with the open-circuit voltage, i.e., with the increase in theoretical capacity, the open-circuit voltage decreases. The In-$MoS_2$ system shows a minimum open-circuit voltage of 0 V; the maximum theoretical capacity is about 650 mAh/g. However, other doped systems of X-$MoS_2$ ($X$ = B, Al, Ga) show a maximum theoretical capacity of more than 700 mAh/g. Similarly, with the group-IVA (C, Si, Ge, Sn) and -VA (N, P, As, Sb) dopants, X-$MoS_2$ substrates show similar trends to those with the group-IIIA dopants. As presented in Figs. 6(b) and 6(c), compared with other elements in the same group, the maximum theoretical capacity of $X$-$MoS_2$ (X = Si, Ge) exceeds 700 mAh/g. Therefore, it can be seen that doped systems of $X$-$MoS_2$ ($X$ = B, Al, Ga, Si, Ge) are very promising high-capacity electrode materials. Considering the previous results that the $X$-$MoS_2$ ($X$ = As, Si, Al) systems have smaller diffusion barriers, we predict that $X$-$MoS_2$ ($X$ = Al, Si) might be good candidates as electrode materials for SIBs with a high rate performance and high theoretical capacity [as shown in Fig. 14 in the Appendix].

## IV. CONCLUSIONS

Based on first-principles calculations, we explore the feasibility of developing 2D $MoS_2$ substrates as electrode materials for Na-ion batteries. The effect of heteroatom doping, charge variation, and the ability to adsorb Na ions are studied systematically. It is found that the $MoS_2$-based systems with suitable empty states near the Fermi level may facilitate the adsorption of Na, which can be tuned by introducing electron-deficient dopants (e.g., group-IIIA, -IVA, and -VA elements) into $MoS_2$.

In addition, the diffusion barrier, theoretical capacity, and open-circuit voltage are examined by doping heteroatoms ($X$ = B, Al, Ga, In, C, Si, Ge, Sn, N, P, As, Sb, O, Se, Te, F, Cl, Br, I) into the $MoS_2$ substrate. It is found that doping can create active centers on the $MoS_2$ substrate, and Na atoms may easily diffuse to the active center. From the potential diffusion profile of Na on $X$-$MoS_2$, we find that the Si-, As-, and Al-doped systems are highly promising electrode materials with the lowest diffusion barrier (~0.1 eV) compared with the other doped systems. The theoretical capacity and open-circuit voltage studies indicate that the B-, Al-, Ga-, Si-, and Ge-doped $MoS_2$ substrate are highly favorable electrode materials for Na-ion batteries. As a result, we predict that the Al- and Si-$MoS_2$ systems can serve as electrode materials for Na-ion batteries, with a high theoretical capacity and high rate performance. These results provide valuable suggestions for experimentalists to design more efficient Na-ion-battery electrode materials with extremely high theoretical capacity.

## ACKNOWLEDGMENTS

This work is supported by the National Natural Science Foundation of China (Grants No. 11874141 and No. U2004212) and Henan Overseas Expertise Introduction Center for Discipline Innovation (Grant No. CXJD2019005). The simulations are performed on resources provided by the High-Performance Computing Center of Henan Normal University.

## APPENDIX: THE STABILITY OF THE $X$-$MoS_2$ STRUCTURES

There are many reports in the literature on the formation energy of the $X$-$MoS_2$ structure and the heteroatoms used in this work. For example, the substitution of Al [41–44], B [44,45], C [46], Si [42,43,45], Ge [47], N [44,48–51], P [42–44,50–52], As [51], O [53], Se [54], Te [55], F [51], Cl [51,56], Br [51], and I [51] atoms for one S atom of $MoS_2$ substrates has been studied from various aspects, and these reports also discuss their stability separately. Among the dopant atoms considered in the present research, only four candidates (Ga, In, Sn, Sb) are not reported.

Since $MoS_2$ materials may easily generate S vacancies in the synthesis process, according to the literature [57–59], the binding energy of the dopant atoms at the S vacancies (defined as $E_{\text{bind}} = E_X + E_{\text{vac - MoS}_2} - E_{X\text{ - MoS}_2}$) in $MoS_2$ is usually used to judge the stability of the dopant atoms. The calculated binding energies shown in Table IV indicate that

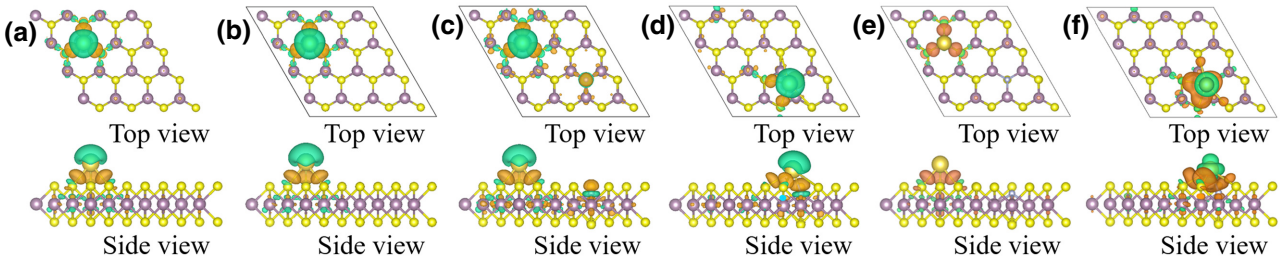


FIG. 7. (a),(b) CDDs of Na atom adsorbed at site 1 on the $MoS_2$ and $MoS_2$ (extract $e$) substrates. (c),(d) CDDs of Na adsorbed at sites 1 and 6 on the N-$MoS_2$ substrate. (e),(f) CDDs of Na adsorbed at sites 1 and 6 on the N-$MoS_2$ (inject $e$) substrate. For contour plots, the green region represents charge depletion, and the orange region represents charge accumulation. Isosurface value of the CDDs is 0.002 e/Å$^3$.

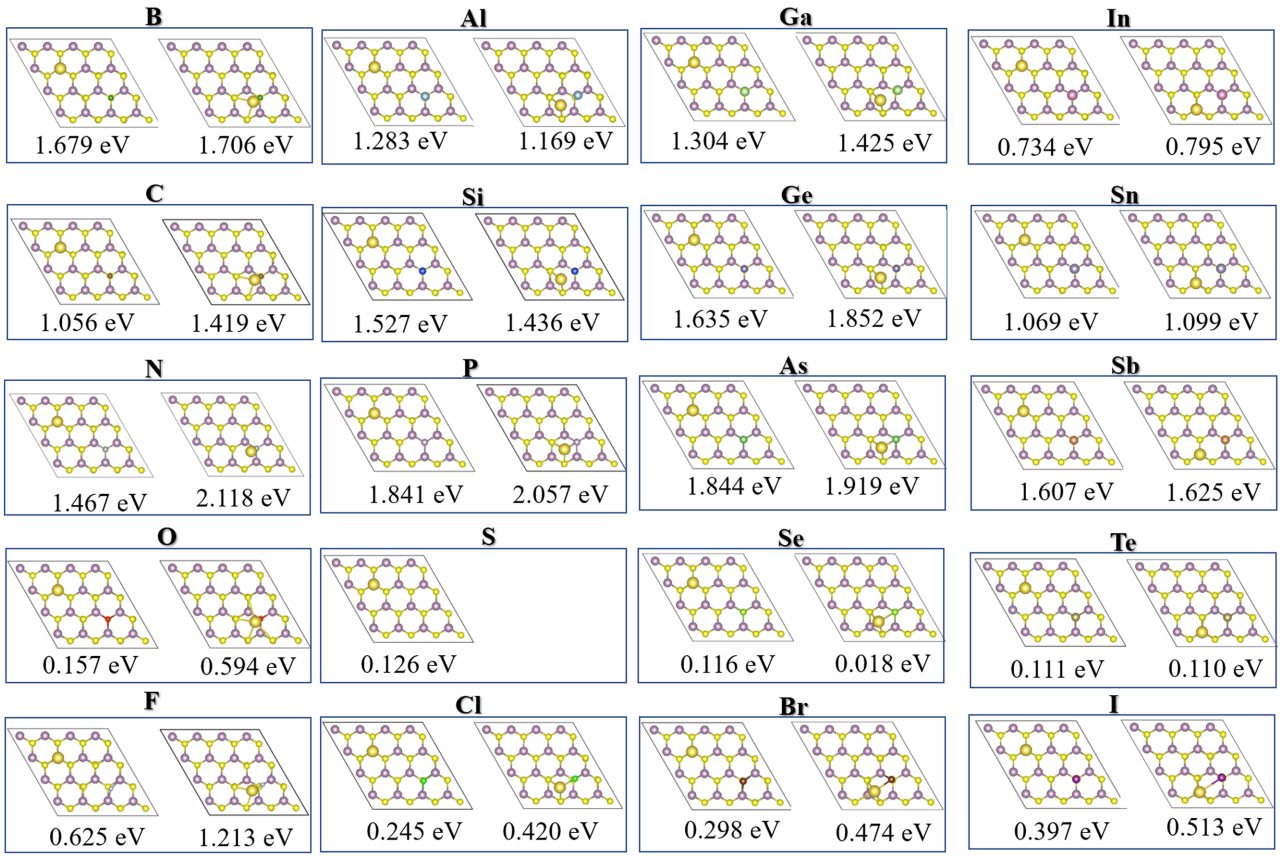


FIG. 8. Optimized structures of $X$-$MoS_2$ ($X$ = B, Al, Ga, In, C, Si, Ge, Sn, N, P, As, Sb, O, Se, Te, F, Cl, Br, I) for different dopant elements and the corresponding adsorption energies of Na.

TABLE II. The adsorption energy of Na at site 1 and site 6 on the $X$-$MoS_2$ substrate ($X$ = B, Al, Ga, In, C, Si, Ge, Sn, N, P, As, Sb, O, Se, Te, F, Cl, Br, I).

| | $E_{ads}$ (eV) | | | $E_{ads}$ (eV) | | | $E_{ads}$ (eV) | | | $E_{ads}$ (eV) | | | $E_{ads}$ (eV) | |
|---|---|---|---|---|---|---|---|---|---|---|---|---|---|---|
| Element | Site 1 | Site 6 | Ele | Site 1 | Site 6 | Ele | Site 1 | Site 6 | Ele | Site 1 | Site 6 | Ele | Site 1 | Site 6 |
| B | 1.68 | 1.71 | C | 1.06 | 1.42 | N | 1.47 | 2.12 | O | 0.16 | 0.59 | F | 0.63 | 1.21 |
| Al | 1.28 | 1.17 | Si | 1.53 | 1.44 | P | 1.84 | 2.06 | S | 0.13 | 0.13 | Cl | 0.25 | 0.42 |
| Ga | 1.30 | 1.43 | Ge | 1.64 | 1.85 | As | 1.84 | 1.92 | Se | 0.12 | 0.02 | Br | 0.30 | 0.47 |
| In | 0.73 | 0.80 | Sn | 1.07 | 1.10 | Sb | 1.61 | 1.63 | Te | 0.11 | 0.11 | I | 0.40 | 0.51 |

the binding of the dopant atoms on vac-$MoS_2$ are all exothermic, with binding energies all greater than 2 eV. While the iodine dopant with a binding energy close to 2 eV is reported to exist stably [51], the stability of the $X$-$MoS_2$ structures can be inferred.

Tables II and III Figures 7–13.

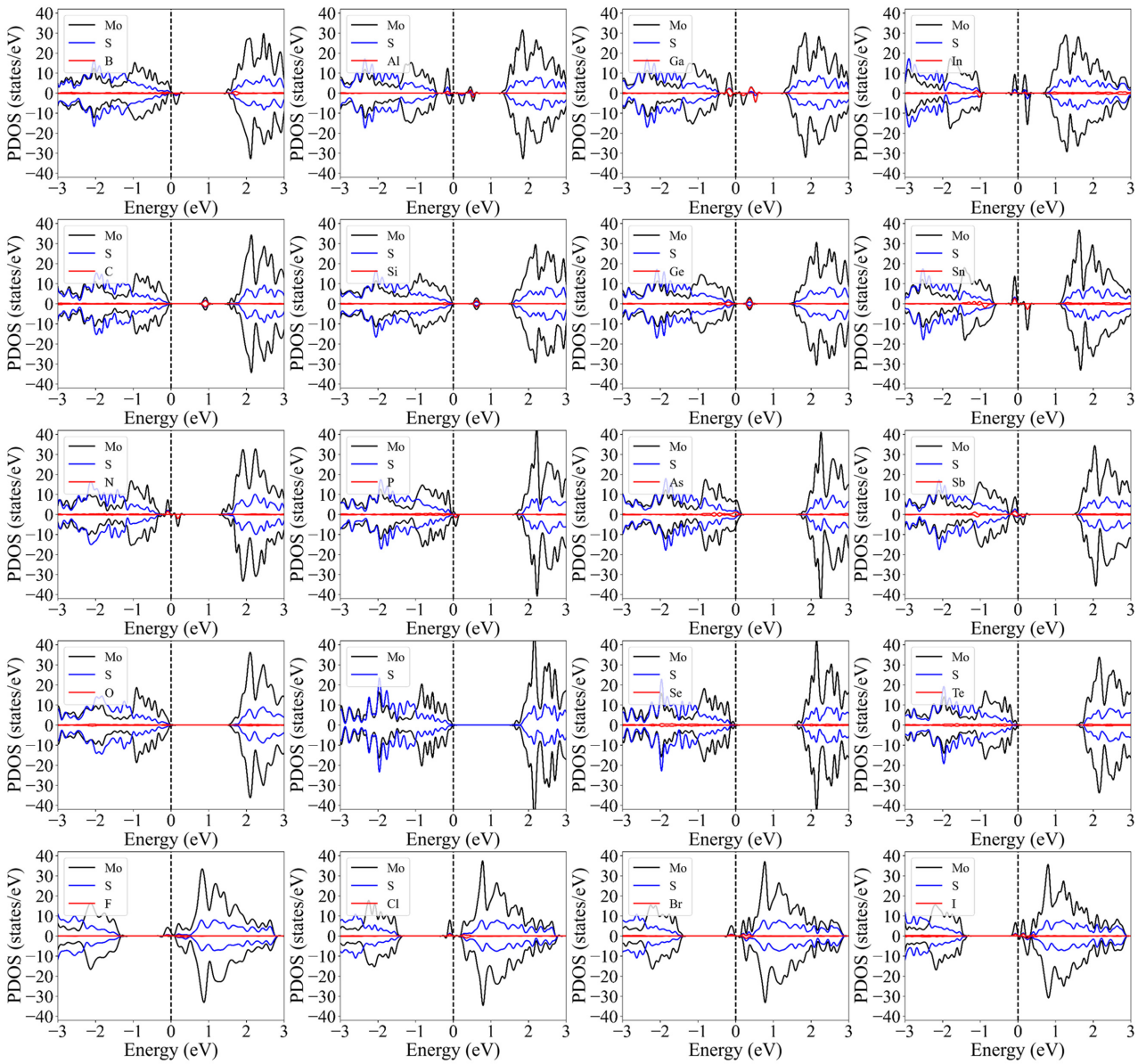


FIG. 9. PDOS of $X$-$MoS_2$ ($X$ = B, Al, Ga, In, C, Si, Ge, Sn, N, P, As, Sb, O, Se, Te, F, Cl, Br, I).

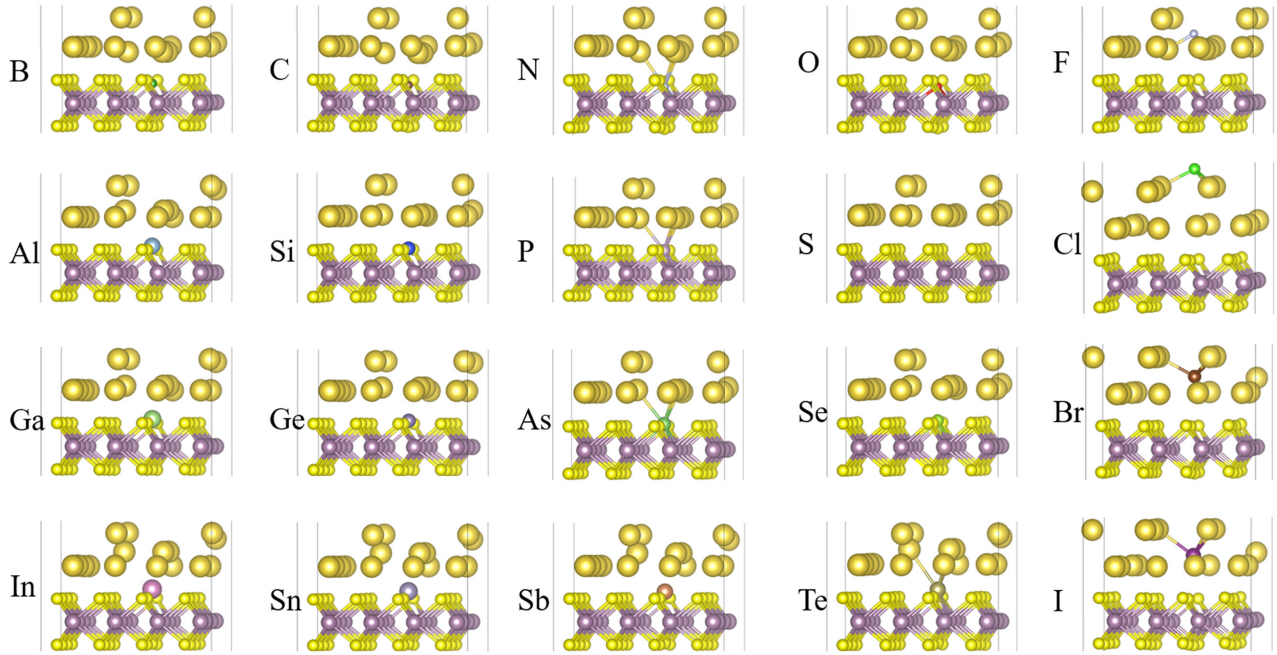


FIG. 10. Multiple Na-adsorption geometries at different sites on $X$-$MoS_2$ substrates ($X$ = doped atoms). Here, a concentration of one monolayer of Na atoms is considered, corresponding to a 1:1 ratio of Na:$MoS_2$.

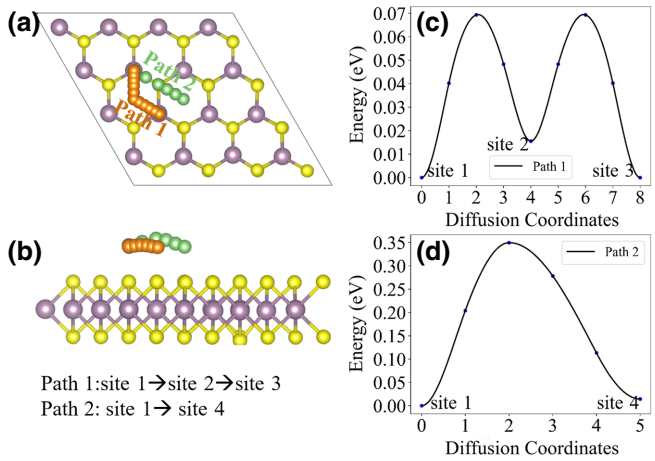


FIG. 11. (a),(b) Top and side views of Na-diffusion path on $MoS_2$ substrate. (c) Corresponding Na diffusion over the $MoS_2$ substrate via path 1. (d) Corresponding Na diffusion over the $MoS_2$ substrate via path 2.

TABLE III. The diffusion barrier of Na on the $X$-$MoS_2$ ($X$ = B, Al, Ga, C, Si, Ge, N, P, As) substrate.

| Element | Diffusion barrier (eV) | Element | Diffusion barrier (eV) | Element | Diffusion barrier (eV) |
|---|---|---|---|---|---|
| B | 0.18 | C | 0.42 | N | 0.68 |
| Al | 0.11 | Si | 0.10 | P | 0.21 |
| Ga | 0.23 | Ge | 0.20 | As | 0.10 |

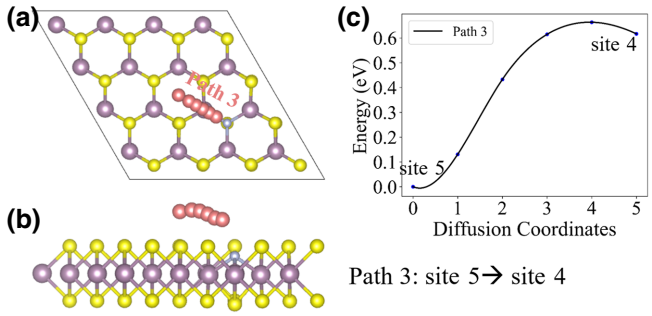


FIG. 12. (a),(b) Top and side views of Na-diffusion path 3 on N-$MoS_2$ substrate. (c) Corresponding Na diffusion over the N-$MoS_2$ substrate via path 3.

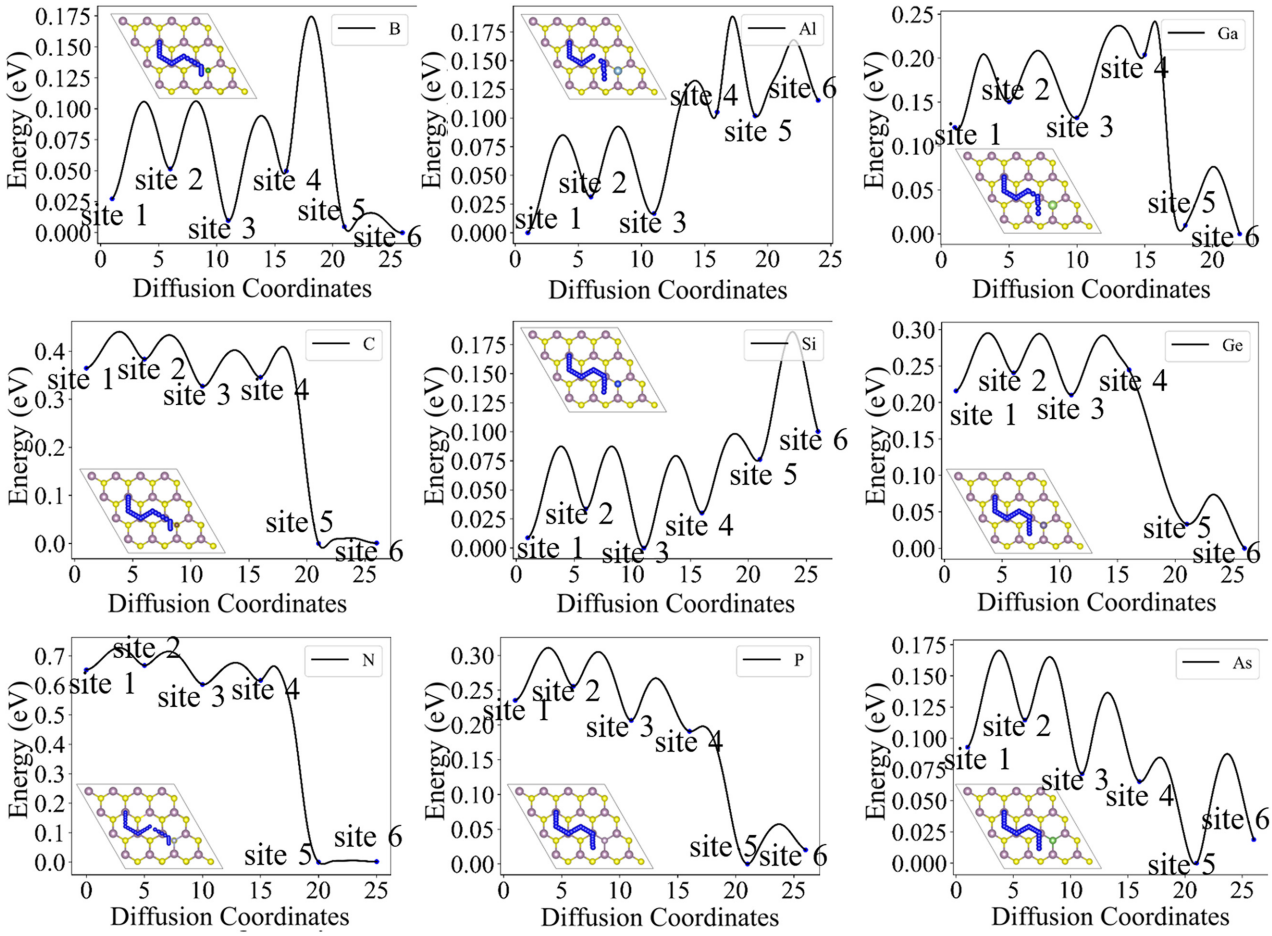


FIG. 13. Diffusion of Na on the $X$-$MoS_2$ ($X = $ B, Al, Ga, C, Si, Ge, N, P, As) substrate.

TABLE IV. The binding energy of the $X$ atom adsorbed on vac-$MoS_2$ ($X = $ doped atoms).

| Element | $E_{bind}$ (eV) | Ele | $E_{bind}$ (eV) | Ele | $E_{bind}$ (eV) | Ele | $E_{bind}$ (eV) | Ele | $E_{bind}$ (eV) | Ele | $E_{bind}$ (eV) |
|---|---|---|---|---|---|---|---|---|---|---|---|
| Li | 2.72 | B | 5.32 | C | 6.99 | N | 6.02 | O | 7.369 | F | 4.38 |
| Na | 2.49 | Al | 2.74 | Si | 4.01 | P | 4.43 | S | 6.08 | Cl | 3.11 |
| Mg | 1.77 | Ga | 2.20 | Ge | 3.14 | As | 3.84 | Se | 8.13 | Br | 2.55 |
| | | In | 2.74 | Sn | 3.44 | Sb | 3.36 | Te | 4.45 | I | 2.01 |

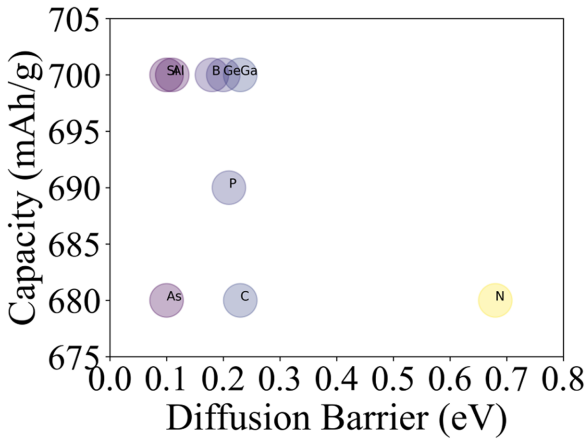


FIG. 14. Relationship between theoretical capacity and barrier.


[1] M. D. Slater, D. Kim, E. Lee, and C. S. Johnson, Sodium-ion batteries, Adv. Funct. Mater. **23**, 947 (2013).

[2] N. Yabuuchi, K. Kubota, M. Dahbi, and S. Komaba, Research development on sodium-ion batteries, Chem. Rev. **114**, 11636 (2014).

[3] J.-Y. Hwang, S.-T. Myung, and Y.-K. Sun, Sodium-ion batteries: Present and future, Chem. Soc. Rev. **46**, 3529 (2017).

[4] C. Vaalma, D. Buchholz, M. Weil, and S. Passerini, A cost and resource analysis of sodium-ion batteries, Nat. Rev. Mater. **3**, 1 (2018).

[5] D. Das, S. Kim, K.-R. Lee, and A. K. Singh, Li diffusion through doped and defected graphene, Phys. Chem. Chem. Phys. **15**, 15128 (2013).

[6] C. Ling and F. Mizuno, Boron-doped graphene as a promising anode for Na-ion batteries, Phys. Chem. Chem. Phys. **16**, 10419 (2014).

[7] H. W. Lee, H. S. Moon, J. Hur, I. T. Kim, M. S. Park, J. M. Yun, K. H. Kim, and S. G. Lee, Mechanism of sodium adsorption on N-doped graphene nanoribbons for sodium ion battery applications: A density functional theory approach, Carbon **119**, 492 (2017).

[8] Y. Yang, D.-M. Tang, C. Zhang, Y. Zhang, Q. Liang, S. Chen, Q. Weng, M. Zhou, Y. Xue, J. Liu, J. Wu, Q. H. Cui, C. Lian, G. Hou, F. Yuan, Y. Bando, D. Golberg, and X. Wang, "Protrusions" or "holes" in graphene: Which is the better choice for sodium ion storage?, Energy Environ. Sci. **10**, 979 (2017).

[9] C. Zhang, Y. Jiao, T. He, F. Ma, L. Kou, T. Liao, S. Bottle, and A. Du, Two-dimensional $GeP_3$ as a high capacity electrode material for Li-ion batteries, Phys. Chem. Chem. Phys. **19**, 25886 (2017).

[10] M. Nasrollahpour, M. Vafaee, M. R. Hosseini, and H. Iravani, Ab initio study of sodium diffusion and adsorption on boron-doped graphyne as promising anode material in sodium-ion batteries, Phys. Chem. Chem. Phys. **20**, 29889 (2018).

[11] Y. Yao, R. Xu, M. Chen, X. Cheng, S. Zeng, D. Li, X. Zhou, X. Wu, and Y. Yu, Encapsulation of $SeS_2$ into nitrogen-doped free-standing carbon nanofiber film enabling long cycle life and high energy density K-$SeS_2$ battery, ACS Nano **13**, 4695 (2019).

[12] Z. Cheng, X. Zhang, H. Zhang, J. Gao, H. Liu, X. Yu, X. Dai, G. Liu, and G. Chen, Prediction of two-dimensional $CP_3$ as a promising electrode material with a record-high capacity for Na ions, Nanoscale Adv. **2**, 5271 (2020).

[13] A. P. Durajski, K. M. Gruszka, and P. Niegodajew, First-principles study of a substitutionally doped phosphorene as anode material for Na-ion batteries, Appl. Surf. Sci. **532**, 147377 (2020).

[14] Z. Cheng, X. Zhang, H. Zhang, J. Gao, H. Liu, X. Yu, X. Dai, G. Liu, and G. Chen, Pentagonal $B_2C$ monolayer with extremely high theoretical capacity for Li-/Na-ion batteries, Phys. Chem. Chem. Phys. **23**, 6278 (2021).

[15] X. Guan, H. Song, Y. Tang, X. Zhong, J. Wang, J. Cheng, and D. Zou, Theory prediction of $PC_3$ monolayer as a promising anode material in potassium-ion batteries, Ionics **27**, 2465 (2021).

[16] J. Hao, Z. Wang, and Y. Wang, High capacity lithium-ion battery anode using silicon-doped blue phosphorene, Superlattices Microstruct. **150**, 106800 (2021).

[17] M. Liu, A. Kutana, Y. Liu, and B. I. Yakobson, First-principles studies of Li nucleation on graphene, J. Phys. Chem. Lett. **5**, 1225 (2014).

[18] H. Yildirim, A. Kinaci, Z.-J. Zhao, M. K. Y. Chan, and J. P. Greeley, First-principles analysis of defect-mediated Li adsorption on graphene, ACS Appl. Mater. Interfaces **6**, 21141 (2014).

[19] M. M. Doeff, Y. Ma, S. J. Visco, and L. C. D. Jonghe, Electrochemical insertion of sodium into carbon, J. Electrochem. Soc. **140**, L169 (1993).

[20] J. R. Dahn and J. A. Seel, Energy and capacity projections for practical dual-graphite cells, J. Electrochem. Soc. **147**, 899 (2000).

[21] Y. Cao, L. Xiao, M. L. Sushko, W. Wang, B. Schwenzer, J. Xiao, Z. Nie, L. V. Saraf, Z. Yang, and J. Liu, Sodium ion insertion in hollow carbon nanowires for battery applications, Nano Lett. **12**, 3783 (2012).

[22] Y. Qiao, R. Han, Y. Pang, Z. Lu, J. Zhao, X. Cheng, H. Zhang, Z. Yang, S. Yang, and Y. Liu, 3D well-ordered porous phosphorus doped carbon as an anode for sodium storage: Structure design, experimental and computational insights, J. Mater. Chem. A **7**, 11400 (2019).

[23] Y. Qiao, J. Wu, X. Cheng, Y. Pang, Z. Lu, X. Lou, Q. Li, J. Zhao, S. Yang, and Y. Liu, Construction of robust coupling interface between $MoS_2$ and nitrogen doped graphene for high performance sodium ion batteries, J. Energy Chem. **48**, 435 (2020).

[24] S. Mukherjee, L. Kavalsky, and C. V. Singh, Ultrahigh storage and fast diffusion of Na and K in blue phosphorene anodes, ACS Appl. Mater. Interfaces **10**, 8630 (2018).

[25] B. Xiao, Y. Li, X. Yu, and J. Cheng, Penta-graphene: A promising anode material as the Li/Na-ion battery with both extremely high theoretical capacity and fast charge/discharge rate, ACS Appl. Mater. Interfaces **8**, 35342 (2016).

[26] G. Barik and S. Pal, Defect induced performance enhancement of monolayer $MoS_2$ for Li- and Na-ion batteries, J. Phys. Chem. C **123**, 21852 (2019).

[27] Y. Feng, M. Xu, T. He, B. Chen, F. Gu, L. Zu, R. Meng, and J. Yang, CoPSe: A new ternary anode material for stable and high-rate sodium/potassium-ion batteries, Adv. Mater. **33**, 2007262 (2021).

[28] Q. Ni, R. Dong, Y. Bai, Z. Wang, H. Ren, S. Sean, F. Wu, H. Xu, and C. Wu, Superior sodium-storage behavior of flexible anatase $TiO_2$ promoted by oxygen vacancies, Energy Storage Mater. **25**, 903 (2020).

[29] B. Radisavljevic, A. Radenovic, J. Brivio, V. Giacometti, and A. Kis, Single-layer $MoS_2$ transistors, Nat. Nanotechnol. **6**, 147 (2011).

[30] Q. Yang, M. Liu, Y. Hu, Y. Xu, L. Kong, and L. Kang, Facile synthesis of $MoS_2$/graphite intercalated composite with enhanced electrochemical performance for sodium ion battery, J. Energy Chem. **27**, 1208 (2018).

[31] G. Kresse and J. Furthmüller, Efficient iterative schemes for *ab initio* total-energy calculations using a plane-wave basis set, Phys. Rev. B **54**, 11169 (1996).

[32] G. Kresse and D. Joubert, From ultrasoft pseudopotentials to the projector augmented-wave method, Phys. Rev. B **59**, 1758 (1999).

[33] P. E. Blöchl, Projector augmented-wave method, Phys. Rev. B **50**, 17953 (1994).

[34] J. P. Perdew, K. Burke, and M. Ernzerhof, Generalized Gradient Approximation Made Simple, Phys. Rev. Lett. **77**, 3865 (1996).

[35] S. Grimme, J. Antony, S. Ehrlich, and H. Krieg, A consistent and accurate *ab initio* parametrization of density functional dispersion correction (DFT-D) for the 94 elements H-Pu, J. Chem. Phys. **132**, 154104 (2010).

[36] S. Grimme, S. Ehrlich, and L. Goerigk, Effect of the damping function in dispersion corrected density functional theory, J. Comput. Chem. **32**, 1456 (2011).

[37] H. J. Monkhorst and J. D. Pack, Special points for Brillouin-zone integrations, Phys. Rev. B **13**, 5188 (1976).

[38] G. Henkelman, A. Arnaldsson, and H. Jónsson, A fast and robust algorithm for bader decomposition of charge density, Comput. Mater. Sci. **36**, 354 (2006).

[39] E. Sanville, S. D. Kenny, R. Smith, and G. Henkelman, Improved grid-based algorithm for Bader charge allocation, J. Comput. Chem. **28**, 899 (2007).

[40] G. Henkelman, B. P. Uberuaga, and H. Jónsson, A climbing image nudged elastic band method for finding saddle points and minimum energy paths, J. Chem. Phys. **113**, 9901 (2000).

[41] M. J. Szary, Al doped $MoS_2$ for adsorption-based water collection, Appl. Surf. Sci. **529**, 147083 (2020).

[42] A. Abbasi, A. Abdelrasoul, and J. J. Sardroodi, Adsorption of CO and NO molecules on Al, P and Si embedded $MoS_2$ nanosheets investigated by DFT calculations, Adsorption **25**, 1001 (2019).

[43] H. Luo, Y. Cao, J. Zhou, J. Feng, J. Cao, and H. Guo, Adsorption of $NO_2$, $NH_3$ on monolayer $MoS_2$ doped with Al, Si, and P: A first-principles study, Chem. Phys. Lett. **643**, 27 (2016).

[44] R. Zhang, D. Fu, J. Ni, C. Sun, and S. Song, Adsorption for $SO_2$ gas molecules on B, N, P and Al doped $MoS_2$: The DFT study, Chem. Phys. Lett. **715**, 273 (2019).

[45] B. Zhao, C. Shang, B. Zhou, R. Q. Zhang, J. J. Wang, Z. Q. Chen, and M. Jiang, Adsorption and dissociation of $H_2O$ molecule on the doped monolayer $MoS_2$ with B/Si, Appl. Surf. Sci. **481**, 994 (2019).

[46] Z. Hai, J. Du, M. K. Akbari, C. Xue, H. Xu, and S. Zhuiykov, Carbon-doped $MoS_2$ nanosheet photocatalysts for efficient degradation of methyl orange, Ionics **23**, 1921 (2017).

[47] J. Xiao, J. Wang, Z. Xue, T. Zhang, J. Wang, and Q. Li, The study of oxygen reduction reaction on Ge-doped $MoS_2$ monolayer based on first principle, Int. J. Energy Res. **45**, 13748 (2021).

[48] P. Liu, Y. Liu, W. Ye, J. Ma, and D. Gao, Flower-like N-doped $MoS_2$ for photocatalytic degradation of RhB by visible light irradiation, Nanotechnology **27**, 225403 (2016).

[49] R. Li, L. Yang, T. Xiong, Y. Wu, L. Cao, D. Yuan, and W. Zhou, Nitrogen doped $MoS_2$ nanosheets synthesized via a low-temperature process as electrocatalysts with enhanced activity for hydrogen evolution reaction, J. Power Sources **356**, 133 (2017).

[50] H. Zhang, Y. Tian, J. Zhao, Q. Cai, and Z. Chen, Small dopants make big differences: Enhanced electrocatalytic performance of $MoS_2$ monolayer for oxygen reduction reaction (ORR) by N- and P-doping, Electrochim. Acta **225**, 543 (2017).

[51] X. Zhao, P. Chen, C. Xia, T. Wang, and X. Dai, Electronic and magnetic properties of $n$-type and $p$-doped $MoS_2$ monolayers, RSC Adv. **6**, 16772 (2016).

[52] H. Huang, X. Feng, C. Du, and W. Song, High-quality phosphorus-doped $MoS_2$ ultrathin nanosheets with amenable ORR catalytic activity, Chem. Commun. **51**, 7903 (2015).

[53] Z. Wei, J. Tang, X. Li, Z. Chi, Y. Wang, Q. Wang, B. Han, N. Li, B. Huang, J. Li, *et al.*, Wafer-scale oxygen-doped $MoS_2$ monolayer, Small Methods **5**, 2100091 (2021).

[54] X. Ren, Q. Ma, H. Fan, L. Pang, Y. Zhang, Y. Yao, X. Ren, and S. (Frank) Liu, A Se-doped $MoS_2$ nanosheet for improved hydrogen evolution reaction, Chem. Commun. **51**, 15997 (2015).

[55] G. H. Oh, S. Kim, and T. Kim, High-performance Te-doped $p$-type $MoS_2$ transistor with high-$K$ insulators, J. Alloys Compd. **860**, 157901 (2021).

[56] T. Kim, Y. Kim, and E. K. Kim, Characteristics of Cl-doped $MoS_2$ field-effect transistors, Sens. Actuators, A **312**, 112165 (2020).

[57] T. Yanase, F. Uehara, I. Naito, T. Nagahama, and T. Shimada, Healing sulfur vacancies in monolayer $MoS_2$ by high-pressure sulfur and selenium annealing: Implication for high-performance transistors, ACS Appl. Nano Mater. **3**, 10462 (2020).

[58] J. Hu, L. Yu, J. Deng, Y. Wang, K. Cheng, C. Ma, Q. Zhang, W. Wen, S. Yu, Y. Pan, *et al.*, Sulfur vacancy-rich $MoS_2$ as a catalyst for the hydrogenation of $CO_2$ to methanol, Nat. Catal. **4**, 3 (2021).

[59] X. Zhang, Q Liao, Z Kang, B Liu, X Liu, Y Ou, J Xiao, J Du, Y Liu, L Gao, *et al.*, Hidden vacancy benefit in monolayer 2D semiconductors, Adv. Mater. **33**, 2007051 (2021).